Impact of the Upstream Plasma Parameters on the Spectroscopic Measurement in the GAMMA 10/PDX Divertor Simulation Experiments*)

Takayuki YOKODO, Yousuke NAKASHIMA, Akiyoshi HATAYAMA[1)], Takaaki IIJIMA, Md. Shahinul ISLAM, Tsubasa YOSHIMOTO, Kazuya ICHIMURA[2)], Md. Maidul ISLAM, Guanyi LEE, Sotaro YAMASHITA, Akihiro TERAKADO, Kunpei NOJIRI, Masayuki YOSHIKAWA, Junko KOHAGURA, Naomichi EZUMI, Mizuki SAKAMOTO and Tsuyoshi IMAI

Plasma Research Center, University of Tsukuba, Tsukuba 305-8577, Japan
[1)]*Graduate School of Science and Technology, Keio University, Yokohama 223-8522, Japan*
[2)]*Graduate School of Engineering, Kobe University, Kobe 657-0013, Japan*

(Received 4 January 2018 / Accepted 19 March 2018)

Detailed results of spectral measurements in the gas injection performed in GAMMA 10/PDX divertor simulation experiments are presented. From the comparison of the emission intensity at the end-cell and plug/barrier-cell, impurity behavior along the magnetic field line is discussed in GAMMA 10/PDX. The emission intensity of Ar II is decreased due to the increase in the background plasma density and the end loss particle flux, which consequently suppresses the Ar particle transport towards the upstream region. The ECH in the plug-cell (EP-ECH) was applied to investigate the influence of the heating on the emission of injected impurities. Ar II intensity slightly increased EP-ECH. On the other hand, Kr II and Xe II decreased at the plug/barrier-cell.

Keywords: GAMMA 10/PDX, divertor, spectroscopic measurement, noble gas, impurity transport

DOI: 10.1585/pfr.13.3402032

1. Introduction

In the nuclear fusion reactor, reduction of high heat and particle fluxes to the target plates of the divertor is one of the important issues. The divertor is exposed to high heat load, and this causes erosion and sputtering at the divertor plates [1]. Therefore, to reduce this heat load, a gaseous divertor concept, called plasma detachment has been suggested. However, radiation losses and dilution in core plasma are mainly caused by impurities [2]. It is important to understand the physical mechanism of impurity transport into the core plasma.

GAMMA 10/PDX consists of the central-cell, anchor-cell, plug/barrier-cell and end-cell. The plasma heating system neutral beam injection (NBI), electron cyclotron resonance heating (ECH) and ion cyclotron range of frequency (ICRF) have been installed in GAMMA 10/PDX [3, 4]. The end loss flux which escapes from the central-cell, has been focused because of applicability and extensibility for studies that require high-performance plasma flux such as plasma-divertor interaction simulation experiments. To make use of high heat flux generated from open magnetic field configuration, the divertor simulation experimental module (D-module) has been installed at the west end-cell. In D-module, a V-shaped target plate made of tungsten is mounted. Various kinds of divertor simulation experiments are available by injecting impurity gases in D-module. Two types of spectrometers, Langmuir probes and calorimeters are installed in the module.

The eventual goal of this study is to reveal the mechanism of radiation cooling, impurity transport and detached plasma formation. To investigate the physics of radiation cooling, various kinds of impurity gases (for example Ar, Kr and Xe) were injected. In the experiment, the light emission result of impurity particles were measured by using spectrometers under several plasma conditions [5]. The particle flux which reaches the end-cell had been changed in three variations. In each variation, impurity gas is injected to compare the influence on the behavior of the impurity emission spectrum observed at D-module and the plug/barrier-cell. The effect of east plug-ECH (EP-ECH) injection on impurities are also investigated from the comparison of the spectral measurement at D-module and the plug/barrier-cell.

2. Experimental Device

GAMMA 10/PDX is the largest tandem mirror device of the total length is 27 m. The volume of the vacuum vessel is 150 m^3. At the central-cell, core plasmas ($T_{i\perp}$ ~4 keV,

author's e-mail: yokodo_takayuki@prc.tsukuba.ac.jp
*) This article is based on the presentation at the 26th International Toki Conference (ITC26).

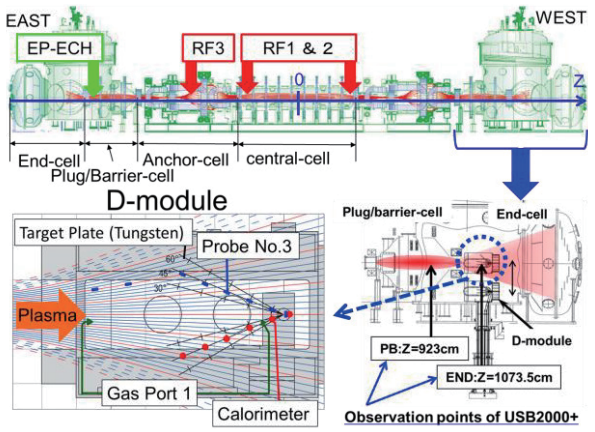

Fig. 1 Schematic view of GAMMA 10/PDX and D-module.

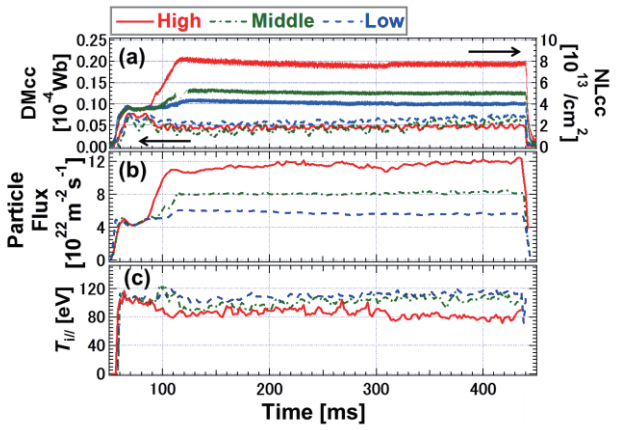

Fig. 2 (a) DMcc and NLcc observed at the central-cell, (b) particle flux and (c) ion temperature observed at the west end-cell.

T_e~100 eV and n_e~10^{18} m^{-3}) are mainly generated by using ICRF (RF1 & 2) and gas puffing. The high temperature of end loss plasma flows from the central-cell to the end-cell. Figure 1 shows the schematic view of GAMMA 10/PDX and D-module. P-ECH is used to form electric potential in the plasma and improve the confinement performance. In D-module, calorimeters which measure the heat flux and Langmuir probes which measure electron temperature and density are installed on the V-shape target plate and at the corner. And those arrays are arranged in parallel to the Z-axis. In this experiment, to measure T_e and n_e, we used Langmuir probe No. 3 which is amounted the closest to the viewpoint of the spectrometer. Three multi-purpose gas injection systems are mounted in D-module. Gas lines are extended from gas bombes through the reservoir tank to the injection ports mounted near the entrance of D-module and under the V-shape target plate.

As diagnostic tools, compact type spectrometer, USB2000+ with wide band-pass (698 nm) is installed at the west anchor-cell, plug/barrier-cell and end-cell. Also, a high wavelength resolution of 0.018 nm FWHM at 372.26 nm and high sensitivity spectrometer (SR500i), is installed at the end-cell. Simultaneous measurements with SR500i and USB2000+ are performed at the end-cell. Only USB2000$^+$ is used at the plug/barrier-cell (Z = 923 cm). In this study, USB2000$^+$ is used with the exposure time of 5 ms to observe a wide range of wavelength.

3. Experimental Results and Discussion

3.1 Particle flux dependence

In the present experiment, the dependence of impurity emission on plasma parameter of the upper-region is investigated. Hydrogen plasma is initiated at t = 50 ms by plasma gun and gas puffing. Plasma is maintained for 400 ms using the ICRF. Particle flux increased by increasing the power of ICRF (RF2 and RF3) and the amount of gas puffing. In Fig. 2 (a), the diamagnetism and electron line-density measured at the central-cell, DMcc and NLcc,

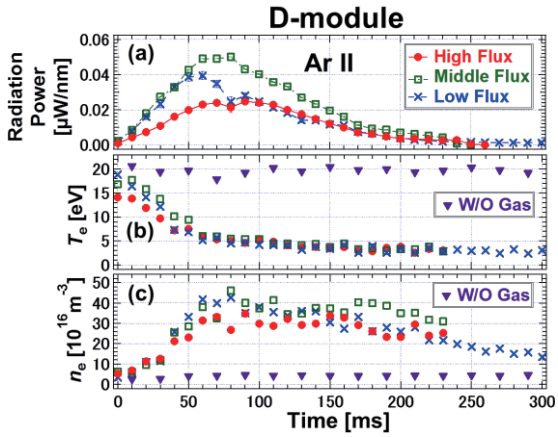

Fig. 3 (a) Ar II (473.59 nm) intensity measured by USB2000+, (b) electron temperature and (c) electron density observed by probe No. 3.

are shown. A gap of NLcc observed in the case of middle flux shown in Fig. 2 (a) is caused by a measurement error of microwave interferometer. The particle flux and $T_{i//}$ were observed by ELIEA [6] mounted at the west end-cell (Figs. 2 (b) and (c)). As NLcc increased, particle flux increased. On the other hand, DMcc was almost the same in all cases. However, $T_{i//}$ had a tendency to decrease with particle flux.

In this experiment, Ar gas was injected at t = 0 s, with the time width of 0.4 s and the plenum pressure was 600 mbar. The plenum pressure is controlled by adjusting the amount of gas in the reservoir tank.

In Fig. 3, the time evolution of Ar II (473.59 nm) intensity (a), T_e (b) and n_e (c) at the nearest probe from the visual field of USB2000+ in D-module are shown. The emission spectra of Ar II once increased in the initial period of the discharge and then decreased. The decrease of Ar II is caused by the monotonical reduction of T_e as shown in Fig. 3 (b) and n_e showed the similar behavior,

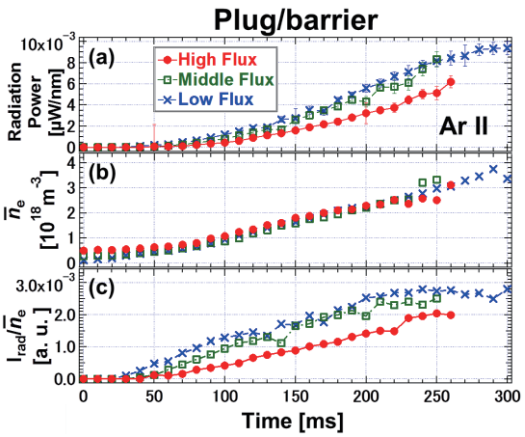

Fig. 4 (a) Ar II (473.59 nm) intensity measured by USB2000+, (b) $\bar{n}_e$ measured by microwave interferometer, (c) $I_{rad}/\bar{n}_e$ calculated from Eq. (1).

which indicates the recombination process is predominant in the last half.

Spectral intensity of Ar II and $\bar{n}_e$ observed at the plug/barrier-cell are shown in Figs. 4 (a) and (b), respectively. Ar II intensity and $\bar{n}_e$ increased monotonically. From the comparison between the highest and the lowest particle flux cases, Ar II intensity decreased according to the increase of particle flux. The increase rate of electron density was high in the low particle flux case and as the time goes by, it got closer to the same value.

In general, spectral intensity I_{rad} can be written as follows,

$$I_{rad} \propto n_Z n_e \langle \sigma v \rangle. \quad (1)$$

The parameters are impurity density n_Z, electron density n_e and rate coefficient $\langle \sigma v \rangle$ which depends on electron temperature. From Eq. (1), $I_{rad}/\bar{n}_e$ is shown in Fig. 4 (c). The difference among three different particle fluxes is clearly demonstrated. The T_e in the plug barrier-cell is $10 \leq T_e \leq 30$ eV, and in this temperature region, the rate coefficient do not change considerably. Therefore, it is suggested that the Ar^+ density became lower as the particle flux increased, which indicate the suppression of Ar^+ transport toward the upstream region.

3.2 Effect of ECH

In order to investigate the effect of ECH on injected impurities, simultaneous measurements by spectrometers are carried out by using USB2000+ along the axis direction. EP-ECH was applied from $t = 300$ ms with a pulse width of 30 ms and the power was 230 kW. The time behavior of DMcc and NLcc observed at the central-cell and the particle flux observed at the west end-cell are shown in Fig. 5. The hatched area represents the time of additional ECH injection. DMcc did not change in both cases. However, NLcc and the particle flux increased.

In this experiment, Ar, Kr and Xe gases are injected

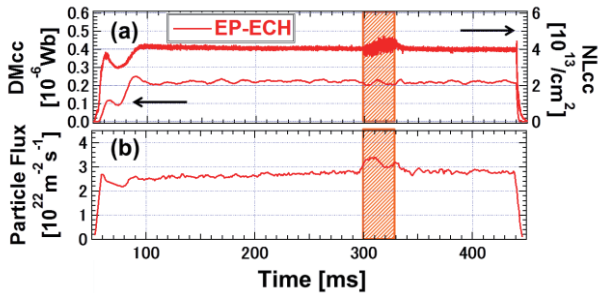

Fig. 5 (a) DMcc and NLcc observed at the central-cell, (b) particle flux observed at the west end-cell.

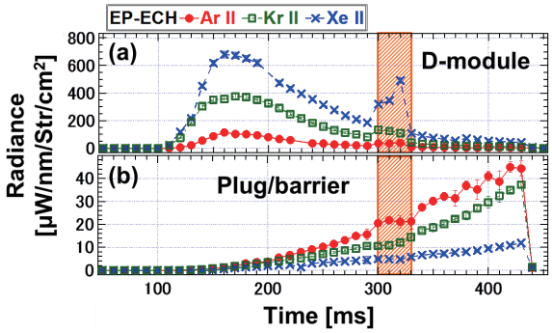

Fig. 6 The emission intensity of Ar II, Kr II and Xe II (a) in D-module and (b) at the plug/barrier-cell in EP-ECH injection experiment.

in the plenum pressure of 600 mbar and the width of 0.4 s. Injection time of Ar was $t = 0.05$ s and the other gas was $t = 0$ s, in order to arrange the timing of gas reaches D-module from the reservoir tank.

In Fig. 6, the time evolution of Ar II (473.59 nm), Kr II (473.9 nm) and Xe II (484.43 nm) measured at D-module (a) and at the plug/barrier-cell (b) are presented in the EP-ECH injection experiment. In D-module, during the EP-ECH injection, the spectral intensity increased in all gas cases. The increase rate was in the order of Xe > Kr > Ar. On the contrary, at the plug/barrier-cell, Ar II slightly increased, however, Kr II and Xe II slightly decreased.

The time evolution of n_e and T_e observed at D-module are shown in Figs. 7 (a) and (b), respectively. During the time of the EP-ECH injection, n_e increased, however, T_e was observed to be kept constant. In this experiment, n_e was not determined partly in the case of Xe gas injection, since the current-voltage characteristics from the probe were not correctly obtained during the EP-ECH. It is considered that the increase of the spectral intensity in D-module with EP-ECH injection is due to the increase of n_e. At the plug/barrier-cell, $I_{rad}/\bar{n}_e$ is calculated from Eq. (1). $I_{rad}/\bar{n}_e$ decreased during the additional heating in all gas cases as shown in Fig. 7 (c). The reduction of $I_{rad}/\bar{n}_e$ was caused by the increase of $\bar{n}_e$ during the EP-ECH injection. This indicates that the impurities moved to higher ionization level, and/or that the impurities flow back to D-

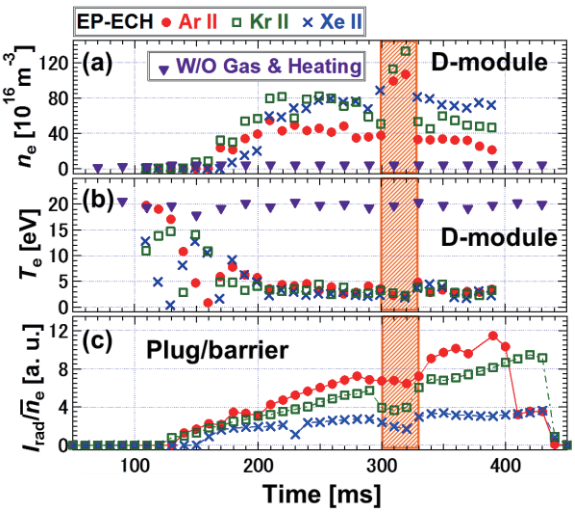

Fig. 7 (a) Electron density and (b) temperature observed by probe No. 3. (c) $I_{rad}/\bar{n}_e$ calculated from Eq. (1).

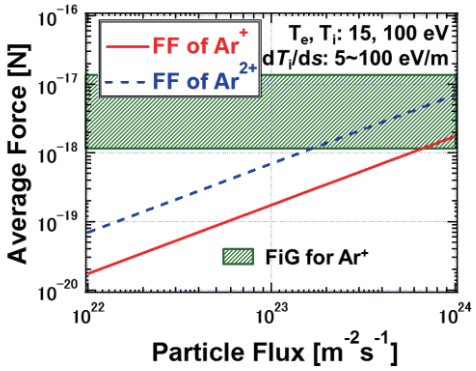

Fig. 8 FF as a function of particle flux and FiG in the range of ion temperature gradient ($d(kT_i/ds)$: 5 ~ 100 eV/m).

module due to the increase of interaction between background plasma and impurity particles. On the other hand, to compare among the behavior of impurity gas species during the EP-ECH, it is considered that not only the difference in ionization energy but also the particle flux effect on different mass impurity is conceivable.

3.3 Discussion

In GAMMA 10/PDX, hydrogen plasma flow is directed toward the target plate in D-module. Also, we assume no flow reversal thus the friction force (FF) is generally toward the target plate [1]. On the other hand, the parallel ion temperature gradient is usually positive, and so ion temperature gradient force (FiG) acts on impurity ions away from the target plate [1].

FF can be expressed by the following formula [1, 7],

$$\mathrm{FF} \equiv m_Z(v_i - v_Z)/\tau_s, \tag{2}$$

where m_Z is the mass of impurity, v_i is the sound speed of background plasma ion parallel to the magnetic field, v_Z is the velocity of impurity ion parallel to the magnetic field and τ_s is the stopping time.

FiG can be represented by [1, 8],

$$\mathrm{FiG} = \beta_i \mathrm{d}(kT_i)/\mathrm{d}s, \tag{3}$$

where β_i is a coefficient which is the order of Z^2. Z is the valency and k is Boltzmann's constant. FF becomes strong as particle flux increases. However, FF weakens as plasma temperature increases, while FiG increases.

From Eqs. (2) and (3), FF is estimated as a function of particle flux between hydrogen for background plasma and Ar^+ for impurity ion as shown in Fig. 8. For the calculation of FF, plasma parameters of $T_e = 15$ eV and $T_i = 100$ eV are given. The green hatched area is the FiG for Ar ion, and it depends on $d(kT_i)/ds$, where $s = 1.5$ m, $Z = 1$ are adopted in the calculation. FF increased as the particle flux increased. From the comparison of these two forces, FiG is stronger than FF in this plasma parameter. The above estimation implies that Ar^+ transported toward the upstream region is mainly caused by FiG. From measured T_i observed at the end-cell was $T_i \leq 120$ eV. From the simulation results [9], T_i and ΔT_i is estimated to be, $T_i \leq 100$ eV and $\Delta T_i < 100$ eV, respectively. From these results, FiG was stronger than FF. However, the effect of mirror force is not contained on the behavior of impurity. In order to investigate the mirror force, we should consider the effect of magnetic field gradient on impurity ions along the axis. In order to resolve the above problem, detailed kinetic simulation by using the IMPGYRO code [10] will be carried out in the future.

4. Summary

In this study, the dependence of particle flux on impurity gas and the effect of ECH are investigated in GAMMA 10/PDX. It is suggested that as the particle flux doubled, the Ar^+ transport toward the upstream region was considered to be suppressed according to the increase of FF. In the experiment of additional heating with EP-ECH to the upstream plasma, it was found that there was a strong influence on the elementary processes of the impurity transport.

For future plans, we will evaluate the pressure gradient force (FPG) to be an influence on impurity ions [1, 7] and will investigate the dependence of gas pressure in D-module by using ASDEX gauge. Measurement of electron temperature at the plug/barrier-cell is also needed in order to reveal the more detail effect of ECH.

Acknowledgments

This study was supported by the bi-directional collaboration research program from the University of Tsukuba and National Institute for Fusion Science (NIFS14KUGM086, NIFS16KUGM117).

[1] P.C. Stangeby, *The Plasma Boundary of Magnetic Fusion*

Devices (IOP publishing, Bristol, 2000).
[2] J. Wesson, *Tokamaks* (Oxford University Press, Oxford).
[3] Y. Nakashima *et al.*, Fusion. Sci. Technol. **68**, 28 (2015).
[4] Y. Nakashima *et al.*, Nucl. Fusion **57**, 116033 (2017).
[5] K. Shimizu *et al.*, Fusion Sci. Technol **68**, 130 (2015).
[6] K. Ichimura *et al.*, Plasma Fusion Res **7**, 2405147 (2012).
[7] S.I. Braginskii, Rev. Plasma Phys. **1**, 205 (1965).
[8] Y. Homma *et al.*, J. Comput. Pys. **231**, 3211 (2012).
[9] M.S. Islam *et al.*, Fusion Eng. Des. **125**, 216 (2017).
[10] A. Fukano *et al.*, J. Nucl. Mater. **363-365**, 211 (2007).